Response of 100% Internal Quantum Efficiency Silicon Photodiodes to 200 eV–40 keV Electrons

H. O. Funsten, *Member, IEEE*, D. M. Suszcynsky, S. M. Ritzau, and R. Korde, *Member, IEEE*

Abstract—Electron irradiation of 100% internal quantum efficiency silicon photodiodes having a thin (60 Å) SiO_2 dead layer results in measured responsivities ranging from 0.056 A/W at an incident electron energy $E_0 = 0.2$ keV to 0.24 A/W at $E_0 = 40$ keV. By comparing the data to a Monte Carlo simulation of electron interactions with the photodiode over an energy range of 1–40 keV, we derive an average electron-hole pair creation energy of 3.71 eV, in close agreement with other studies. Analysis of electron energy lost to processes that do not contribute to electron-hole pair creation shows that the energy lost in the SiO_2 dead layer is dominant for $E_0 < 1.5$ keV, whereas the energy removed by backscattered electrons is dominant for $E_0 > 1.5$ keV. At $E_0 = 300$ eV, the Monte Carlo simulation results show that the electron projected range is significantly less than the dead layer thickness even though the measured response is 0.082 A/W, indicating that electron-hole pairs generated in the oxide dead layer are collected by the junction.

Index Terms— Charge carrier processes, dielectric radiation effects, electron detectors, electron radiation effects, photodiodes, radiation effects, silicon radiation detectors.

I. INTRODUCTION

RECENT technological developments have yielded silicon photodiodes with 100% internal quantum efficiency having a thin (40–80 Å) SiO_2 passivation layer that enables near-theoretical quantum efficiencies for EUV photons [1]–[3]. These photodiodes can be used for precise EUV measurements for fusion experiment diagnostics, laboratory plasma analysis, and space-based EUV detection, for example on the space shuttle, SOHO, and GOES [4].

In contrast to traditional solid state detectors having a thick window that stops low-energy (a few keV) particles, plasma ions and electrons with sufficient energy can transit the thin dead layer of these photodiodes and induce a photodiode current. While the presence of these particles introduces an error when using the photodiodes to measure EUV photons, these photodiodes provide a unique capability for direct measurement of low-energy plasma particles.
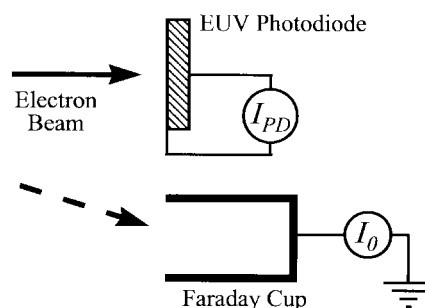
Fig. 1. The experimental apparatus used to measure the incident electron beam current and the photodiode current during electron irradiation.

In this study, we have measured and modeled the response of these photodiodes to 0.2–40 keV electrons. The experimental procedure, in which we measure the photodiode current induced by an electron beam with a measured energy and beam current, is similar to the measurement of the pulse magnitudes of individual high-energy ions or electrons striking surface barrier detectors [5]–[7] and measurement of the electron beam-induced current (EBIC), which is a standard technique used to characterize semiconductor materials and devices [8]–[10]. Using these techniques as a basis, we model the deviation of the measured response of the photodiode from its theoretical response based on the average electron-hole pair creation energy by characterizing energy loss mechanisms in which the incident electrons lose energy that does not contribute to electron-hole pair creation.

II. EXPERIMENTAL METHOD

Fig. 1 shows the method used to measure the photodiode response to electrons. An electron beam with energy E_0 was first directed into a Faraday cup, and the incident beam current I_0 was measured. The beam was then directed onto the photodiode, which was operated without bias, and the photodiode current I_{PD} was measured. To ensure beam stability during the measurement of I_{PD}, the beam current was measured a second time, and I_0 was taken as the average of the two beam current measurements.

Two different apparatuses were used to generate the appropriate electron beam: a low-energy electron gun that produced electrons with energies ranging from 0.2 to 4 keV and a scanning electron microscope (SEM) that generated electrons with energies ranging from 4 to 40 keV.
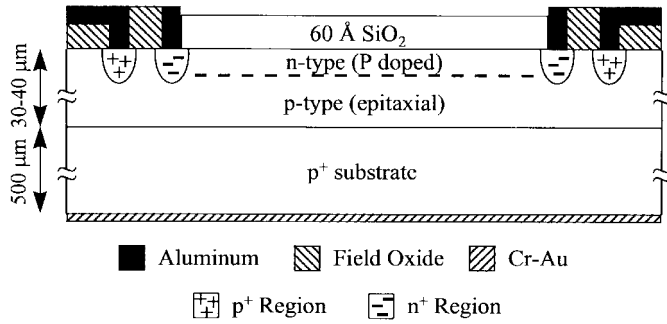
Fig. 2.   Schematic of 100% internal quantum efficiency silicon photodiode.
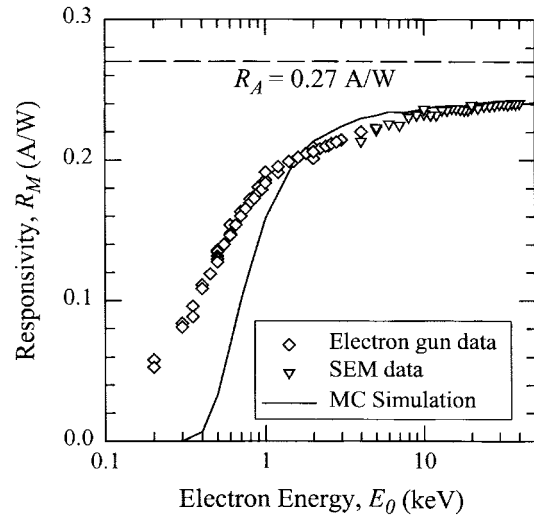

Fig. 3.   Photodiode responsivity from 0.2 to 40 keV electrons: experimental data (symbols), Monte Carlo simulation (solid line), and average responsivity for Si (dashed line).

The electron beam produced by the low-energy electron gun had a diameter of 2.5 mm and a stability better than $\pm 1\%$ over all measurements. During electron irradiation of the photodiode, the photodiode was exposed to the filament of the electron gun and detected the filament's photon emission. This photocurrent, I_{PHOTON}, which was measured by turning the electron accelerating voltage to 0 V so that electrons are not accelerated into the photodiode, was stable to within $\pm 0.01\%$. During electron irradiation, we measured the total photodiode current I_{TOT}, from which we derived the photodiode current due to the electrons according to $I_{\mathrm{PD}} = I_{\mathrm{TOT}} - I_{\mathrm{PHOTON}}$. Typically, $I_{\mathrm{PHOTON}} \approx 700$ nA, $I_0 \approx 120$ pA, and I_{PD} ranged from 5 to 100 nA.

For electrons with energies 4–40 keV, the SEM provided convenient and precise control of the electron beam parameters, including the spot size and the spot location. This enabled quantification of the dependence of the response on the electron flux. For these measurements, the spot size was 5×5 μm, I_0 ranged from 15 pA to 2.5 nA and remained stable to within $\pm 3\%$ for all measurements, and I_{PD} ranged from 10 nA to 24 μA.

The silicon photodiodes, which had an active area of 1 cm^2, are illustrated schematically in Fig. 2. They were fabricated using p–p$^+$ epitaxial silicon wafers. The p$^+$ channel stop and an n$^+$ guard ring were produced by diffusions before the active area formation. Subsequently, the ~ 0.1 μm active area n-type layer was created by phosphorus diffusion doping, followed by the thermal growth of an ~ 60-Å SiO$_2$ passivating layer. These diodes do not have a doped dead-region and have zero surface recombination, resulting in 100% internal quantum efficiency for EUV, near UV, and visible photons. These characteristics also enable detection of incident electrons that can traverse the 60 Å SiO$_2$ dead layer.

III. RESULTS

We define the measured responsivity R_{M} as

$$R_{\mathrm{M}} = \frac{I_{\mathrm{PD}}}{I_0(E_0/e)} \qquad (1)$$

which utilizes the electron charge e and the measured values I_{PD}, I_0, and E_0. Fig. 3 shows the measured responsivity R_{M} of the photodiodes derived using the low-energy electron gun (diamonds) and the SEM (triangles). The measured responsivity equals ~ 0.24 A/W at electron energies greater than 20 keV, and R_{M} decreases with decreasing E_0.

R_{M} is less than the responsivity $R_{\mathrm{A}} \approx 0.27$ A/W that is derived from the average electron-hole pair creation energy $\varepsilon_{\mathrm{A}} \approx 3.7$ eV [8] in silicon. The deviation of R_{M} from R_{A} results from electron energy loss to processes that do not lead to electron-hole pair creation or from electron-hole recombination in the photodiode. These processes include energy loss by incident electrons in the dead layer, energy removed by backscattered electrons, and residual energy losses, which primarily consists of recombination of electron-hole pairs created in the depletion region. We define the fraction of the incident beam energy contributing to these processes as the dead layer loss Δ_{DL}, the backscatter loss Δ_{B}, and the residual loss Δ_{R}. The observed responsivity is, therefore

$$R_{\mathrm{M}} = R_{\mathrm{A}}(1 - \Delta_{\mathrm{DL}} - \Delta_{\mathrm{B}} - \Delta_{\mathrm{R}} + \Gamma). \qquad (2)$$

We include Γ to account for the larger responsivity that is observed at lower energies compared to the modeled values. If no energy losses are present, then $R_{\mathrm{M}} \approx R_{\mathrm{A}}$; if the total loss $\Delta_{\mathrm{DL}} + \Delta_{\mathrm{B}} + \Delta_{\mathrm{R}}$ is significant, then $R_{\mathrm{M}} \ll R_{\mathrm{A}}$.

A. Dead Layer Loss, Δ_{DL}

Particles transiting the 60 Å SiO$_2$ dead layer of the photodiode lose energy, and this energy loss is assumed here to produce no electron-hole pairs that contribute to the observed photodiode current I_{PD}. The dead layer loss, which equals the fraction of the incident energy lost in the dead layer, is

$$\Delta_{\mathrm{DL}} = \frac{c(E)}{E_0} \int_w \frac{dE}{ds}\, ds \qquad (3)$$

where dE/ds is the stopping power of the incident particle in SiO$_2$ and the integral of dE/ds represents the total energy lost by the particle over its pathlength w in the dead layer.

Since the integral of dE/ds is expressed as the average energy loss per incident electron in the dead layer, the factor $c(E)$ accounts for backscattered particles that can lose a different amount of energy in the dead layer than the average energy loss described by the integral of dE/ds. For example,

this can result from electrons backscattered in the depletion region that transit the dead layer twice or from electrons that backscatter near the surface of the dead layer and therefore lose little energy in the dead layer.

At keV energies, electrons undergo few scatter events in the dead layer, so w is approximately equal to the dead layer thickness. At lower energies, the number of electron scattering events in the dead layer can be large, so w can be much greater than the dead layer thickness.

B. Backscatter Loss, Δ_B

A significant fraction of incident electrons can be backscattered from the photodiode. By defining the backscatter coefficient η and the average energy $\overline{E}_B$ of a backscattered electron, we represent the backscatter loss as the fraction of the incident energy removed by backscattered electrons as

$$\Delta_B = \frac{\eta \overline{E}_B}{E_0}. \tag{4}$$

As will be shown in Section IV, Δ_B is the most significant loss mechanism for $E_0 > 1.5$ keV.

C. Residual Loss, Δ_R

The residual loss Δ_R consists of all other energy losses not included in Δ_{DL} or Δ_B that act to decrease the responsivity. Typically, a significant contribution to Δ_R is electron-hole recombination within or at the boundaries of the active area of the detector. We note that recombination losses form the basis of EBIC characterization of semiconductor devices [8]–[10], and quantification of residual losses is crucial for accurate energy measurements of individual high-energy ions and electrons detected with silicon surface-barrier detectors [11], [12].

Recombination of electron-hole pairs created in the depletion region can arise from two sources. First, recombination centers in the depletion region or at the Si–SiO$_2$ interface can reduce the photodiode current. However, the photodiodes used here are known to have 100% internal quantum efficiency, indicating the absence of recombination centers. Second, recombination can occur from a high-density plasma formed, for example, by high-energy ion irradiation, high flux electron bombardment, or a small electric field across the depletion region of the device [9], [11]–[14]. Following a simplified model derived by Finch *et al.* [12], which overestimates recombination by not considering the expansion of the initial ionization along the ionization track of the incident particle, we estimate the recombination loss to be 5×10^{-4} for the experimental method and electron energies used in this study. This will not be observed within the experimental error of the data.

Using the SEM, we observed no statistically significant dependence of R_M on the beam current or beam current density of the incident electron beam. We conclude that recombination of electron-hole pairs created in the depletion region is small, so Δ_R can be neglected. We therefore only consider Δ_{DL} and Δ_B.
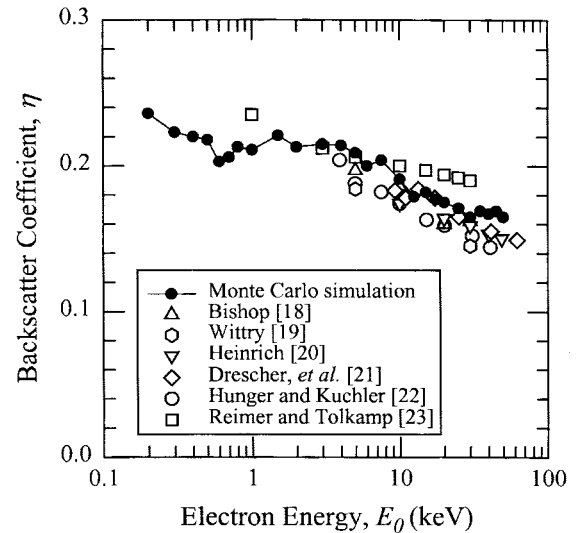

Fig. 4. Backscatter coefficient from experimental data (open symbols) [18]–[23] and the Monte Carlo simulation (points). For $E_0 > 1$ keV, the simulations agree with the data.

IV. MONTE CARLO SIMULATION OF THE PHOTODIODE RESPONSE

To model the electron interaction with the photodiode, we use a Monte Carlo simulation [15] that follows individual electrons as they interact with a solid. The simulation employs a modified Bethe continuous slow-down approximation [16] to calculate energy loss and screened Rutherford scattering. We construct a 60-Å-thick SiO$_2$ layer on a Si substrate and track the energy lost by incident electrons in the dead layer and depletion region in addition to the fraction (η) and average energy ($\overline{E}_B$) of backscattered electrons. For the SiO$_2$ layer, the Monte Carlo simulation utilized an average atomic number and atomic mass weighted according to the stoichiometry (i.e., $Z = 10$ and an atomic mass of $A = 20$) [17]. Each simulation consisted of 10^4 incident electrons.

Fig. 4 shows the backscatter coefficient from the photodiode structure that was derived using the Monte Carlo simulation. For comparison, measured backscatter yields [18]–[23] from Si targets are shown as open symbols. The simulation results, in which η ranges from 0.24 at 0.2 keV to 0.16 at 50 keV, agree with the measured values for incident electron energies greater than several keV. At this higher energy range, we expect good agreement with measured backscatter yields since the dead layer thickness is much less than the projected range of the electrons, so that most backscattered electrons originate from the Si depletion region rather than from the SiO$_2$ dead layer.

Fig. 5 illustrates the ratio $\overline{E}_B/E_0$, which is the average fraction of the incident energy that is carried away by electrons backscattered from the photodiode structure. The variation of $\overline{E}_B/E_0$ with incident energy is small, ranging from approximately 0.6 at 0.2 keV to 0.63 at 50 keV.

Using (4) with the values of η and $\overline{E}_B/E_0$ derived from the Monte Carlo simulations, we obtain the backscatter loss Δ_B, illustrated in Fig. 6, which linearly decreases from 0.16 at 200 keV to 0.10 at 50 keV. Also shown in Fig. 6 is the
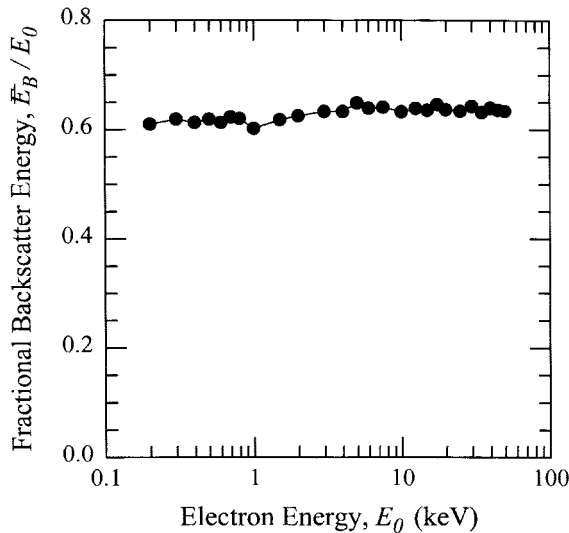
Fig. 5. The average backscattered electron energy, derived using the Monte Carlo simulation and normalized to the incident energy, is a slowly increasing function of energy.
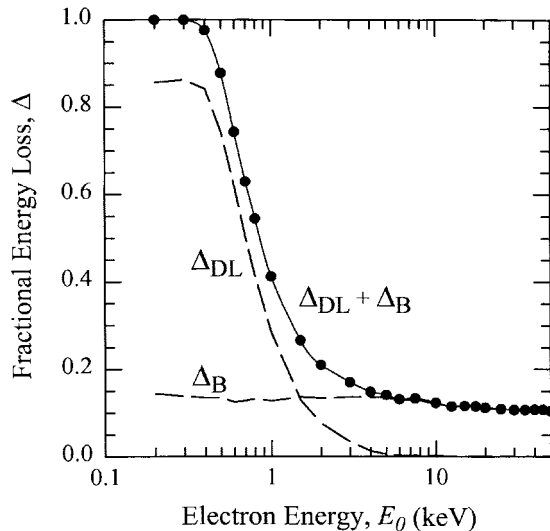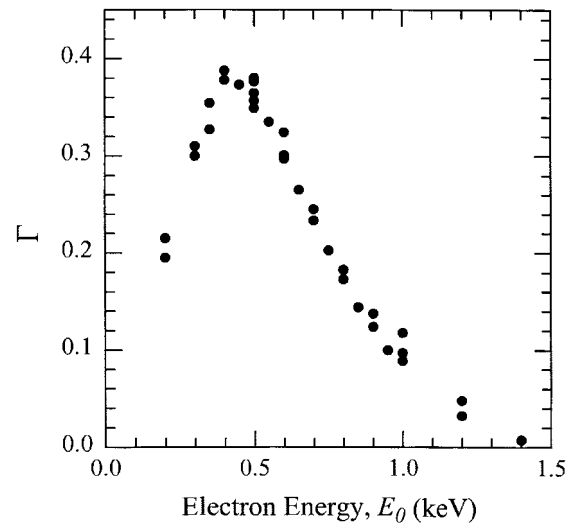

Fig. 7. Enhancement of the measured responsivity compared to that derived using the Monte Carlo simulation is shown as a function of energy. These results indicate that electron-hole pairs created in the dead layer can diffuse to the depletion region, where they are collected and measured.

Also depicted in Fig. 6 is the total loss $\Delta_B + \Delta_{DL}$ that is predicted by the Monte Carlo simulation. For $E_0 > 5$ keV, this total loss equals the backscatter loss. Since $\Delta_B + \Delta_{DL} = 1$ for $E_0 \leq 0.3$ keV, the responsivity should equal zero according to (2).

Fig. 6. Beam energy carried away by backscattered electrons (quantified by the backscatter loss Δ_B) and energy loss in the dead layer (quantified by the dead layer loss Δ_{DL}) cause the measured responsivity to be less than $R_A = 0.27$ A/W, which is based on the average electron-hole pair creation energy $\varepsilon_A \approx 3.7$ eV in Si. The Monte Carlo simulation predicts no electrons traverse the dead layer for $E_0 \leq 0.3$ keV.

V. DISCUSSION

We derive the responsivity R_A, which corresponds to the average electron-hole pair creation energy in Si, by equating (2) to the measured values of R_M for $E_0 \geq 20$ keV, using the total loss $\Delta_B + \Delta_{DL}$ derived using the Monte Carlo simulation, and assuming $\Gamma = 0$. We obtain $R_A = 0.270$ A/W for Si. This corresponds to an electron-hole pair creation energy in Si of $\varepsilon_A = 3.71$ eV, which agrees well with other values ranging from 3.61–3.79 eV that were derived using high-energy alpha and beta particles (see Wu and Wittry [8] and references therein). In particular, this agrees closely with an EBIC study using 20–50 keV electrons that derived $\varepsilon_A = 3.75$ eV [8].

Using (2) with the derived value $R_A = 0.270$ A/W and the total loss $\Delta_B + \Delta_{DL}$ from the Monte Carlo simulation, we obtain the modeled responsivity that is shown as the solid line in Fig. 3. For $E_0 \geq 1.5$ keV the modeled responsivity agrees closely with the measured values. However, it clearly deviates from the measured values for $E_0 \leq 1$ keV, and for $E_0 \leq 0.3$ keV the simulation predicts that no electrons will enter the depletion region which contradicts the measured responsivity of >0.05.

We use Γ to quantify the deviation between the measured and modeled responsivity that is observed at lower energies. We derive Γ using (2) with $R_A = 0.270$ A/W, and the losses Δ_B and Δ_{DL} computed using the Monte Carlo simulation. The resulting values of Γ depicted in Fig. 7 show an increase in the deviation with increasing energy to a maximum value $\Gamma = 0.38$ at approximately 0.5 keV and a subsequent decrease toward a value of $\Gamma = 0$ at 1.5 keV.

dead layer loss Δ_{DL}, which corresponds to the fraction of the incident beam energy that is lost in the SiO_2 dead layer of the photodiode structure.

The magnitudes of the dead layer and backscatter losses are equivalent at 1.5 keV. As E_0 decreases below 1.5 keV, Δ_{DL} rapidly increases and reaches a constant value for $E_0 \leq 0.3$ keV, at which point no energy is deposited in the depletion layer.

The backscatter loss slowly decreases with increasing energy, which results from the decreasing backscatter coefficient. For $E_0 \geq 5$ keV, the simulation results show that $\Delta_B \gg \Delta_{DL}$ and indicate that electrons interact predominantly with the depletion region instead of the dead layer.

We interpret this enhanced responsivity as diffusion of electron-hole pairs created in the dead layer to the depletion region, where they are collected and contribute to the photodiode current. A similar effect has been observed in photodiodes exposed to photons that are strongly absorbed in the SiO_2 dead layer [3]. Since Γ is dependent on the depth distribution of electron-hole pair production and the diffusion of holes and electrons into the depletion region, we can qualitatively discuss the general shape of Γ by reasonably assuming that electrons and holes that enter the depletion region must be created in the dead layer close to the Si–SiO_2 interface. For $E_0 > 0.5$ keV, Γ decreases nearly linearly with increasing energy and corresponds to less energy deposited in the dead layer as the electrons penetrate deeper into the photodiode. For $E_0 < 0.5$ keV, the decrease in Γ likely results from energy deposited farther from the Si–SiO_2 interface and closer to the surface of the window, where recombination may be more efficient and the diffusion path of electrons and holes to the depletion region is longer.

VI. CONCLUSION

The response of 100% internal quantum efficiency photodiodes to low-energy electrons has been measured and modeled using a Monte Carlo simulation. By comparing the measured responsivity to the modeled responsivity, we derive an average electron-hole creation energy of 3.71 eV for Si, which agrees closely with other studies. The simulation results show removal of beam power by backscattered electrons is the primary loss mechanism that reduces the measured responsivity for energies greater than 1.5 keV, whereas the dead layer loss is the dominant loss mechanism for lower energies. At lower incident electron energies, we attribute the higher measured responsivity compared to the calculated values to electrons and holes that are created in the dead layer and diffuse into the depletion region, where they are collected and measured as a component of the photodiode current.

REFERENCES

[1] R. Korde and J. Geist, "Quantum efficiency stability of silicon photodiodes," *Appl. Opt.,* vol. 26, pp. 5284–5290, 1989.
[2] R. Korde, J. S. Cable, and L. R. Canfield, "One gigarad passivating nitrided oxides for 100% internal quantum efficiency silicon photodiodes," *IEEE Trans. Nucl. Sci.,* vol. 40, pp. 1655–1669, Dec. 1993.
[3] L. R. Canfield, J. Kerner, and R. Korde, "Stability and quantum efficiency performance of silicon photodiode detectors in the far ultraviolet," *Appl. Opt.,* vol. 28, no. 18, pp. 3940–3943, 1989.
[4] R. Korde and L. R. Canfield, "Silicon photodiodes with stable, near theoretical quantum efficiency in the soft x-ray region," in *Proc. SPIE, Symp. X-Ray Instrum. Medicine Biology, Plasma Phys., Astrophys., and Synchrotron Radiation,* 1989, vol. 1140, pp. 126–132.
[5] R. H. Pehl, F. S. Goulding, D. A. Landis, and M. Lenzlinger, "Accurate determination of the ionization energy in semiconduction detectors," in *Semiconductor Nuclear-Particle Detectors and Circuits,* W. L. Brown, W. A. Higinbotham, G. L. Miller, and R. L. Chase, Eds. Washington, DC: National Acad. Sci., 1969, pp. 19–36.
[6] B. D. Wilkins, M. J. Fluss, S. B. Kaufman, C. E. Gross, and E. P. Steinberg, "Pulse-height defects for heavy ions in a silicon surface-barrier detector," *Nucl. Instrum. Methods,* vol. 92, pp. 381–391, 1971.
[7] H. Funaki, M. Mashimo, M. Shimizu, Y. Oguri, and E. Arai, "Pulse height defect of low energy ions in surface barrier detectors," *Nucl. Instrum. Methods Phys. Res. B,* vol. 56, pp. 975–977, 1991.
[8] C. J. Wu and D. B. Wittry, "Investigation of minority-carrier diffusion lengths by electron bombardment of Schottky barriers," *J. Appl. Phys.,* vol. 49, no. 5, pp. 2827–2836, 1978.
[9] H. J. Leamy, "Charge collection scanning electron microscopy," *J. Appl. Phys.,* vol. 53, no. 6, pp. R51–R80, 1982.
[10] D. B. Holt, "The conductive mode," in *SEM Microcharacterization of Semi-Conductors,* D. B. Holt and D. C. Joy, Eds. London, U.K.: Academic, 1989, pp. 241–338.
[11] E. P. Steinberg, S. B. Kaufman, B. D. Wilkins, C. E. Cross, and M. J. Fluss, "Pulse height response characteristics for heavy ions in silicon surface-barrier detectors," *Nucl. Instrum. Methods,* vol. 99, pp. 309–320, 1972.
[12] E. C. Finch, M. Asghar, and M. Forte, "Plasma and recombination effects in the fission fragment pulse height defect in a surface barrier detector," *Nucl. Instrum. Methods,* vol. 163, pp. 467–477, 1979.
[13] M. Ogihara, Y. Nagashima, W. Galster, and T. Mikumo, "Systematic measurements of pulse height defects for heavy ions in surface-barrier detectors," *Nucl. Instrum. Methods,* vol. A251, pp. 313–320, 1986.
[14] E. C. Finch, "Systematic measurements of pulse height defects for heavy ions in surface-barrier detectors—A comment," *Nucl. Instrum. Methods,* vol. A257, pp. 381–383, 1987.
[15] D. C. Joy, *Monte Carlo Modeling for Electron Microscopy and Microanalysis.* New York: Oxford, 1995.
[16] D. C. Joy and S. Luo, "An empirical stopping power relationship for low-energy electrons," *Scanning,* vol. 11, pp. 176–180, 1989.
[17] R. H. Müller, "Interaction of beta particles with matter," *Phys. Rev.,* vol. 93, pp. 891–892, 1954.
[18] H. E. Bishop, "Some electron backscattering measurements," in *X-Ray Optics and Microanalysis,* R. Castaing, P. Deschamps, and J. Philibert, Eds. Paris: Hermann, 1966, vol. 4, pp. 153–158.
[19] D. B. Wittry, "Secondary electron emission in the electron probe," in *X-Ray Optics and Microanalysis,* R. Castaing, P. Deschamps, and J. Philibert, Eds. Paris: Hermann, 1966, vol. 4, pp. 168–180.
[20] K. F. J. Heinrich, "Electron probe microanalysis by specimen current measurement," in *X-Ray Optics and Microanalysis,* R. Castaing, P. Deschamps, and J. Philibert, Eds. Paris: Hermann, 1966, vol. 4, pp. 159–167.
[21] H. Drescher, L. Reimer, and M. Seidel, "Rückstreukoeffizient und sekundärelektronen-ausbeute von 10–100 keV-elektronen und beziehungen zur raster-elektronenmikroskopie," *Z. Angew. Phys.,* vol. 29, pp. 331–336, 1970.
[22] H.-J. Hunger and L. Küchler, "Measurements of the electron backscattering coefficient for quantitative EPMA in the energy range of 4 to 40 keV," *Phys. Status Solidi (a),* vol. 56, pp. K45–K48, 1979.
[23] L. Reimer and C. Tollkamp, "Measuring the back-scattered coefficient and secondary electron yield inside a scanning electron microscope," *Scanning,* vol. 3, pp. 35–39, 1980.